

# All-Optical Segmentation via Diffractive Neural Networks for Autonomous Driving

Yingjie Li<sup>\*+</sup>

*Simon Fraser University*

yingjie\_li@sfu.ca

Daniel Robinson\*

*Massachusetts Institute of Technology*

daniel\_r@mit.edu

Cunxi Yu

*University of Maryland, College Park*

cunxiyu@umd.edu

**Abstract**—Semantic segmentation and lane detection are crucial tasks in autonomous driving systems. Conventional approaches predominantly rely on deep neural networks (DNNs), which incur high energy costs due to extensive analog-to-digital conversions and large-scale image computations required for low-latency, real-time responses. Diffractive optical neural networks (DONNs) have shown promising advantages over conventional DNNs on digital or optoelectronic computing platforms in energy efficiency. By performing all-optical image processing via light diffraction at the speed of light, DONNs save computation energy costs while reducing the overhead associated with analog-to-digital conversions by all-optical encoding and computing. In this work, we propose a novel all-optical computing framework for RGB image segmentation and lane detection in autonomous driving applications. Our experimental results demonstrate the effectiveness of the DONN system for image segmentation on the CityScapes dataset. Additionally, we conduct case studies on lane detection using a customized indoor track dataset and simulated driving scenarios in CARLA, where we further evaluate the model’s generalizability under diverse environmental conditions.

**Index Terms**—Diffractive optical neural network, semantic segmentation, lane detection, autonomous driving

## I. INTRODUCTION

Autonomous driving represents one of the most transformative innovations in modern transportation. Autonomous driving is designed to perceive the environment, make decisions, and navigate roads with minimal human intervention. The development of autonomous driving systems not only benefits people’s daily life but also shows the potential to enhance the road safety and improve the traffic efficiency. Autonomous driving has become one of the most actively researched and rapidly evolving fields with widespread attention from both academia [8], [22] and industry [10], [25].

Within an autonomous driving system, the environment is first sensed by delicate sensors such as cameras, LiDAR, radar, etc. Then the sensor data is combined to create an accurate environment model. The environment is then analyzed by perception models, which are typically deep-learning based models, to build a complete scene understanding for the vehicle. After predictions and planning with the analyzed information from perception models, controls are generated to physically move the vehicle along the planned path [39]. During the process, the sensed information is converted to

digital format and fed to digital systems for processing. The design of the perception model with the sensor data is critical in autonomous driving. Many deep learning frameworks have been proposed as the perception models for reliable and energy-efficient perception in all environments and conditions, providing efficient and real-time response (autonomous control generation) to the environment [11], [35], [36].

However, the communication and memory access with digital processors are energy consuming, and can cause significant latency [15]. Moreover, digital DNN frameworks require substantial computational efforts and expensive memory usage to achieve high performance, posing further challenges for edge computing and power management during the deployment of autonomous vehicles [23].

To enhance the efficiency of autonomous driving systems, it is important to improve the latency and the computational efficiency of large-scale digital DNNs. There has been a growing trend towards developing novel high-performance while energy-efficient DNNs platforms, especially implementing novel DNNs in the optical domain, e.g., optical neural networks (ONNs), that mimic conventional feed-forward neural network functions using light propagation [7], [14], [29]. Free-space Diffractive Optical Neural Networks (DONNs) is a promising research area in ONNs for autonomous driving in that: **(1)** Different from digital computing platforms and integrated photonics-based optoelectronic systems that demand preprocessed inputs, free-space DONN systems have direct access to all the optical degrees of freedom that carry information about an input scene/object without needing digital recovery or preprocessing of information. **(2)** DONNs feature with its high system throughput, inherent parallel processing and fast computation speeds with minimal power consumption by enabling all-optical inference through passive optical devices. DONNs realize all-optical computation by manipulating the information carrier, light signal, with physical phenomena such as light diffraction and phase modulation, which occur by nature at the speed of light in the medium, while requiring no additional energy for computation.

To bring the advantages of DONN systems into autonomous driving applications, we propose a novel DONN architecture designed for image segmentation and lane detection tasks in this work. Our main contributions are as follows:

- We introduce a novel DONN architecture for all-optical

<sup>+</sup>: Corresponding author: Yingjie Li (yingjie\_li@sfu.ca).

<sup>\*</sup>: Work done when study at the University of Utah.

RGB images processing, demonstrating with image segmentation and lane detection tasks in autonomous driving. The architecture is designed with three separate channels, each dedicated to processing the red ("R"), green ("G"), and blue ("B") components of an RGB environment input. We incorporate optical skip connections between the early layers and the predication layers within each channel to address the vanishing gradient problem and achieve effective model training.

- We provide a comprehensive analysis of the proposed model for the image segmentation task using CityScapes dataset [1]. Our results show that our architecture delivers more detailed and accurate segmentation compared to the existing DONN system [14].
- We evaluate the model's performance in lane detection tasks through two case studies: track trace extraction for robotic cars in an indoor playground, and lane extraction for urban scenes simulated in CARLA [3]. Additionally, we demonstrate the model's generalizability across different maps, weather conditions, and times of the day.

## II. BACKGROUND AND RELATED WORKS

### A. Deep Learning for Autonomous Driving

Autonomous driving (AD) has been a prominent research topic in recent years, and it gets lots of attention and practical applications through the use of deep learning systems. There are mainly four steps involved in enabling autonomous driving: (1) Sensor data acquisition and fusion, where the vehicle's sensors continuously capture data from the surrounding environment. The vehicle is typically equipped with multiple kinds of sensors, such as cameras, LiDAR, radar, and GPS, to capture comprehensive environment information. The sensor data is then fused to generate an accurate model of the environment; (2) Perception, where deep learning models are employed to interpret the surrounding environment. Key tasks for the perception model include object detection, semantic segmentation, and lane detection; (3) Predictions and planning, where the vehicle predicts the future movements of other agents and plans its own movement to ensure safe driving; (4) Control generation, where the control signal is generated to physically move the vehicle along the planned path. The ultimate goal for autonomous driving is to realize safe, reliable, and energy-efficient driving that outperforms human drivers in all environments and conditions [37].

Developing high-fidelity and generalizable deep learning models for perception tasks is critical in autonomous driving assistance systems [27]. The first deep learning models used for semantic segmentation perform pixel-wise classification on the input image based on the feature extraction of the input image using convolutional models, including Fully Convolutional Network (FCN) [17], VGG [30], ResNet [5], and MobileNet [6]. Novel network architectures designed specifically for semantic segmentation are then proposed. For example, ParseNet [16] adds global context to the deep learning network, and DeconvNet [24] incorporates deconvolution and unpooling layers to improve the performance. Recently, attention-based models

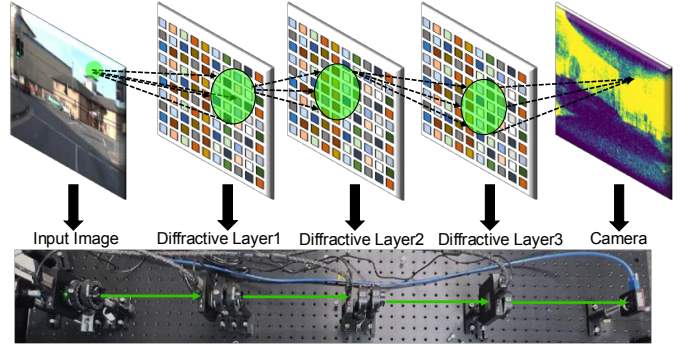


Fig. 1: The basic DONN framework. The upper part illustrates the extracted model for a DONN system including the input image, three diffractive layers, and the system output for the image segmentation task. The lower part shows the hardware deployment for the all-optical inference with a trained DONN system. It includes a laser source for input image encoding and computation, three SLMs for diffractive layers, and a camera to capture the system output.

have gained significant attention. Based on the transformer architecture [34], the Vision Transformers (ViT) [2] is proposed for image understanding, which presents a convolution-free, transformer-based vision approach.

In autonomous driving, perception models must not only be accurate but also maintain low inference times to ensure real-time responses. Additionally, as the deep learning model is deployed on edge computing platforms in autonomous vehicles that are resource-constrained, energy efficiency of the model is crucial for practical deployment. However, existing digital deep learning models are complex and requires heavy computation involving millions of neurons. This results in high power consumption and expensive memory requirements, posing significant challenges for efficient deployment.

### B. Optical Computing Systems

In the past decade, there has been an increasing interest in optical computing platforms because of their potential to realize fast, massively parallel computation at low power consumption [31]. There are two main directions to bring the advantages of optics into the computing paradigm: (1) integrated photonics-based optical systems, which integrate optical computing units with digital systems to accelerate the computing speed while reducing the energy cost. This approach requires massive conversions between digital and analog signal for information inputs, computing, and outputs; (2) free-space diffractive optical systems, which have direct access to all optical degrees of freedom that carry information of the analog input wave without the requirement of analog-to-digital conversions (ADCs), further saving the energy cost while maintaining more accurate input information.

1) *Integrated Photonics-based Optical Processor* : Integrated photonics-based processors [29] are designed and implemented with on-chip interferometers and waveguide-embedded light sources to replace or empower their electronic counterparts. They work as an efficient on-chip task-specific

accelerator in a whole computing system with their reconfigurability and ease of integration with electronics, making them powerful and versatile for optoelectronic computing.

However, the computing systems integrated with photonic devices often require pre-processing of information with ADCs/DACs, which can be energy-costly. In the optoelectronic computing system, nearly 50% of power is from electrical memory, and ADCs/DACs take another 20-30%, while the photonic circuit consumes less than 10% total power [26]. The speed and power consumption for memory and ADCs/DACs determine the overall benefits the computing system could gain from the integration with optical accelerators.

2) *Free-space Diffractive Optical Neural Networks (DONNs)*: Unlike digital NNs and integrated photonics-based optical computing systems, DONNs take the direct optical information as system inputs for computing without requiring input pre-processing, offering an efficient solution to further improve the perception performance for autonomous driving. The DONN system performs all-optical inference for ML tasks based on physical phenomena by manipulating the light signal's features, such as phase and amplitude, with passive optical devices. Thus, the DONN system features high system throughput, high computation speed, while having low power consumption [9], [14], [29]. As shown in Figure 1, in the DONN system, the information is encoded onto the light signal emitted by a laser source, through modulation methods. Multiple diffractive layers are employed to manipulate features of the light signal, such as its phase and amplitude. These layers are implemented with spatial light modulators (SLMs). The layers form the neural network and each pixel in the layer acts as a neuron, which mimic the morphology of artificial neural network with passive optical devices, while requiring no additional energy for computation [19], [20]. At the end of the system, a detector is used to capture the results. Compared to digital NNs, the DONN system encodes weights as complex-valued transmission coefficients (phase modulation to the light signal) within the diffractive layers. The free-space light diffraction provides neuron connectivity across neighboring layers with forward propagation within the DONN system.

Existing DONN systems are typically implemented with single channel, restricting their applications to grayscale input images only [14], [32]. Additionally, existing DONN systems are primarily used for classification tasks with one-hot represented labels [13], [14], [38], [40], limiting applications to more complex image processing tasks. In this work, we propose a novel DONN architecture designed for advanced RGB image processing tasks including image segmentation and lane detection. Our framework takes an image as input and produces a processed image as output, expanding the functionality of DONNs beyond simple classification.

### III. APPROACH

In this section, we introduce a novel DONN architecture to process RGB images for semantic image segmentation. To train a DONN model for machine learning tasks, the optical

responses during the all-optical inference by DONN systems is first emulated on digital platforms with numerical modeling. The training process leading the design of a functioning DONN system is performed on digital platforms with the mathematical approximation of the system.

#### A. Numerical Modeling of DONN Systems for RGB Images

The model structure is illustrated in Figure 2a. Targeting RGB images, we build three channels in the DONN system for "R", "G", and "B" image components respectively. (1) The "R", "G", and "B" image components of the RGB input are obtained after the optical sensor captures incoming light and the optical passive filter spatially separates it into red ("R"), green ("G"), and blue ("B") components. The sensed data is used to configure/fabricate the "Encode Layers" for each component in each channel. (2) The three grayscale input image information for each component is then encoded on the coherent laser light signal. The laser beam is splitted into three sub-beams with same intensity by beam splitters, where the half-wave plate is used to decay the intensity of one of the sub-beams by half for even light intensity distribution over all channels. The image information for each component is encoded on the laser beam for each channel with "Encoding Layers". (3) For each channel, there are separate diffractive layers to manipulate the information-encoded light signal within the channel. The light signal is diffracted in the free space between diffractive layers, and modulated via phase modulation at each layer. (4) Finally, the diffraction patterns after light propagation regarding light intensity distribution from all three channels are mixed and captured at the detector plane as the processed image output by the DONN system.

1) *Forward Function for DONN Systems*: For each channel, the input information (e.g., "R" component image) is encoded on the coherent light signal, where the light signal is expressed with complex-valued numbers in the DONN emulation. Its wavefunction after the encoding layer is expressed as  $f^0(x_0, y_0)$ . The wavefunction after light diffraction over diffraction distance  $z$  to the first diffractive layer can be seen as the summation of the outputs at the input plane, i.e.,

$$f^1(x, y) = \iint f^0(x_0, y_0)h(x - x_0, y - y_0, z)dx_0dy_0 \quad (1)$$

where  $(x, y)$  is the coordinate on the receive plane, and  $h$  is the impulse optical response function of free space, which is the mathematical approximation for light diffraction, e.g., Rayleigh-Sommerfeld approximation, Fresnel approximation, Fraunhofer approximation [33], resulting in the non-trainable parameters in DONN systems. For example, in this work, we use Fresnel approximation for DONN emulation, where

$$h(x, y, z) = \frac{\exp(ikz)}{i\lambda z} \exp\left\{\frac{ik}{2z}(x^2 + y^2)\right\} \quad (2)$$

where  $i = \sqrt{-1}$ ,  $\lambda$  is the wavelength of the laser source,  $k = 2\pi/\lambda$  is free-space wavenumber.

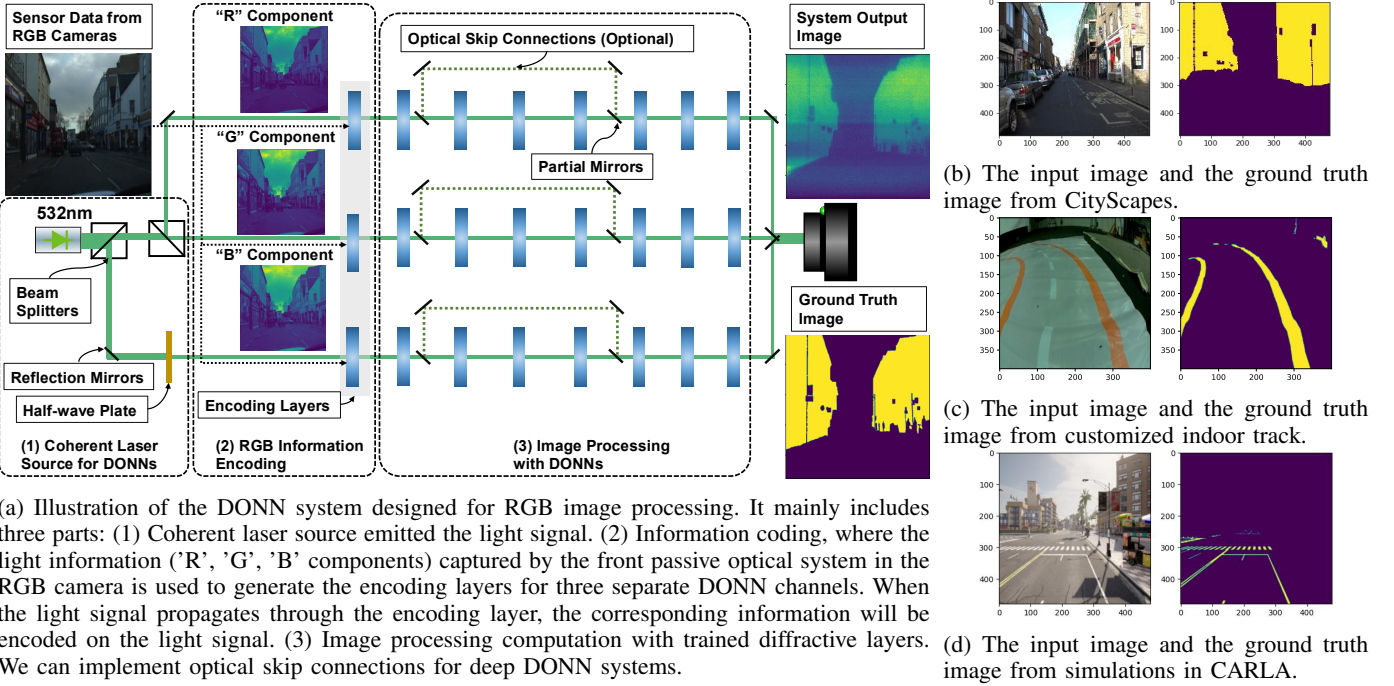


Fig. 2: Illustrations of the DONN system for image segmentation and lane detection with RGB images.

Equation 1 can be calculated with spectral algorithm, where we employ Fast Fourier Transform (FFT) for fast and differentiable computation, i.e.,

$$U^1(\alpha, \beta) = U^0(\alpha, \beta)H(\alpha, \beta, z) \quad (3)$$

where  $U$  and  $H$  are Fourier transformations of  $f$  and  $h$ , respectively.

After light diffraction, the resulting wavefunction  $U^1(\alpha, \beta)$  in Equation 3 is transformed to time domain with inverse FFT (iFFT) for phase modulation, and the phase modulation  $W(x, y)$  provided by the diffractive layer is applied to the light wavefunction by matrix multiplication, i.e.,

$$f^2(x, y) = \text{iFFT}(U^1(\alpha, \beta)) \times W_1(x, y) \quad (4)$$

where  $W_1(x, y)$  is the phase modulation in the first diffractive layer,  $f^2(x, y)$  is then the input light wavefunction for the light diffraction for the second diffractive layer.

We wrap one computation round of light diffraction and phase modulation at one diffractive layer as a computation module named **DiffMod**, i.e.,

$$\text{DiffMod}(f(x, y), W) = L(f(x, y), z) \times W(x, y) \quad (5)$$

where  $f(x, y)$  is the input wavefunction,  $W(x, y)$  is the phase modulation,  $L(f(x, y), z)$  is the wavefunction after light diffraction over a constant distance  $z$  in time domain.

Thus, in a multiple diffractive layer constructed DONN system, the forward function  $f^*$  can be computed iteratively for the stacked diffractive layers. For example, for a 3-layer constructed channel in the system, the forward function is

$$f^*(f^0(x, y), W) = \text{DiffMod}(\text{DiffMod}(\text{DiffMod}(f^0(x, y), W_1), W_2), W_3) \quad (6)$$

**2) Optical Skip Connections Between Diffractive Layers:** Adopted from residual neural networks [5], we implement the optical skip connection into the DONN system to recover the vanishing gradients for effective model training in deep systems. **However, the optical skip connection involves free-space light diffraction during the propagation through the skip distance between layers.**

As shown in Figure 2a, an optical skip connection is implemented after the first computing layer and before the fifth computing layer in (3). The distance between each layer is  $z$ , the propagation distance for the optical skip connection is thus  $4 \times z$ . When the wavefunction of the light signal after propagating through the first layers is  $f_1^*$  and the wavefunction of the light signal after the fourth layers is  $f_4^*$ , the wavefunction of the input light signal to the fifth layer  $f_5^0$  is

$$f_5^0 = f_4^* + L(f_1^*, 4 \times z) \quad (7)$$

Thus, the forward function with the optical skip connection in Figure 2a is

$$\begin{aligned} f^*(f_0(x, y), \mathbf{W}) &= \text{DiffMod}(\text{DiffMod}(\text{DiffMod}(\text{DiffMod}(f_0(x, y), \mathbf{W}_1), \mathbf{W}_2), \mathbf{W}_3) \\ &\quad ((\text{DiffMod}(\text{DiffMod}(\text{DiffMod}(f_0(x, y), \mathbf{W}_1), \mathbf{W}_2), \mathbf{W}_3) \\ &\quad \mathbf{W}_4) + L(f_1^*, 4 \times z), \mathbf{W}_5), \mathbf{W}_6), \mathbf{W}_7) \end{aligned} \quad (8)$$

Note that we can insert optical skip connections between arbitrary layers while setting the corresponding skip distance for light diffraction. The optical skip connections can be implemented with passive optical devices including partial mirrors and reflection mirrors as shown in Figure 2a, which requires no extra energy cost.

3) **Light Intensity at the Detector:** The wavefunction  $f^*$  is a complex-valued number and it can be represented by  $f^* = A + iB$ , where  $A$  and  $B$  are real numbers. Thus, the output intensity pattern is expressed as

$$I = A^2 + B^2 \quad (9)$$

The modeling for each channel is following the same numerical emulation as shown in Equation 8 and 9. The forward function  $I$  for the "R", "G", "B" channels can be expressed with  $I_R$ ,  $I_G$ ,  $I_B$ , where the inputs  $f^0(x, y)$  are the corresponding input  $f_{R/G/B}^0(x, y)$  from the 'R/G/B' component, and  $W$  are the corresponding phase modulations  $W_{R/G/B}$  trained separately in each channel. The final diffraction pattern at the detector of this three-channel RGB-image segmentation DONN framework is expressed as

$$I_{det} = I_R + I_G + I_B \quad (10)$$

where  $I_{det}$  is the intensity pattern captured at the detector.

### B. Dataset Processing

In this work, the ground truth images in datasets are preprocessed as binary images for image segmentation task and lane detection task. Specifically, we utilize three datasets in this work: (1) CityScapes dataset [1], which captures complex urban scenes and is used for segmentation tasks. In this work, we modify its labels by making it binary such that building pixels are marked as "1"s and non-building pixels are marked as "0"s, as shown in Figure 2b. (2) Indoor track detection dataset. We record the video with a robotic car driving along a real-world indoor track. Each frame is extracted from the video and manually annotated to build the dataset. As shown in Figure 2c, we annotate the tracks as "1"s, while others are marked as "0"s. (3) Simulated driving dataset. This dataset includes simulated urban driving scenes generated in CARLA [3]. As shown in Figure 2d, the pixels for lane markers on the road are set as "1"s while others are set as "0"s.

### C. Model Training

The all-optical DONN system is trained with the numerical modeling as shown in Equation 8, 9, and 10 on digital platforms. The trainable parameters in the system are the phase modulation  $W$  provided at each diffractive layer. By manipulating the phase of the information-encoded light signal at each diffractive layer during light propagation, the final diffraction pattern changes accordingly, and the system output is produced by reading the final intensity pattern on the camera. Hence, similar to the training process of conventional DNNs, optimal phase modulation in diffractive layers in DONN can be obtained by minimizing the commonly used machine learning loss functions [14].

The ground truth of the segmented image is first processed as binarized images as described in Section III-B. The intensity distribution for the ground truth image is  $I_{GT}$  as shown in Figure 2b to 2d. With the output from the DONN system expressed with Equation 10, we implement the loss function

between the ground truth image ( $I_{GT}$ ) and the system output  $I_{det}$ . Then, we apply Mean Square Error (MSE) loss between  $I_{GT}$  and  $I_{det}$ , the loss function  $L$  is calculated as

$$\mathcal{L}_{MSE} = \frac{1}{N^2} \sum_{i=1}^N \sum_{j=1}^N (I_{GT}^{ij} - I_{det}^{ij})^2 \quad (11)$$

Moreover, we can implement different loss functions for the training such as Binary Cross-Entropy (BCE) loss and Dice loss [21]. The explorations regarding different training loss functions are shown in Section IV-B2. Thus, the whole system is designed to be differentiable and compatible with conventional automatic differential engines.

## IV. EXPERIMENTS

This section presents the evaluations of the proposed DONN system for image segmentation task and lane detection task in autonomous driving. First, Section IV-B provides the evaluations on the image segmentation task with the CityScapes dataset, including model explorations and the performance comparisons with existing image segmentation systems [14], [28]. Then, the model is evaluated with lane detection task in Section IV-C with the customized indoor track dataset and the simulated driving dataset with CARLA. The generalizability of the model is also explored with different environment conditions with the dataset from CARLA.

### A. Experiments Setups

Our DONN systems are implemented with three channels for RGB input images. For different tasks with different datasets, the DONN system is prepared with different setups. For the image segmentation task with CityScapes dataset in Section IV-B, where the input samples are more complex, we set system size as  $480 \times 480$ . The comparison and explorations are conducted with the system implemented with fifteen diffraction layers and three optical skip connections between the first layer and the fifteenth layer, the second layer and the fourteenth layer, and the third layer and the thirteenth layer for each separate channel. For the lane detection task with the indoor customized track dataset in Section IV-C, where the input samples are clean and minimalistic, featuring a well-defined object against a plain background, the input image and the system size is set as  $400 \times 400$ . The DONN system is implemented with eight diffraction layers and three optical skip connections between the first layer and the sixth layer, the second layer and the seventh layer, and the third layer and the eighth layer, for each each channel. The same system architecture is used for lane detection with the simulated driving dataset with CARLA in Section IV-C, while the system size is set to  $480 \times 480$ . The Intersection over Union (IoU) is used as the metric to evaluate the segmentation performance. The IoU is calculated between the binary ground truth image and the binarized output image from the DONN system.

The input information is encoded on the coherent light signal with the wavelength of  $532\text{ nm}$ . The pixel size for each diffractive layer is  $36\text{ }\mu\text{m}$ . The physical distances between layers, first layer to source, and final layer to detector, are set as

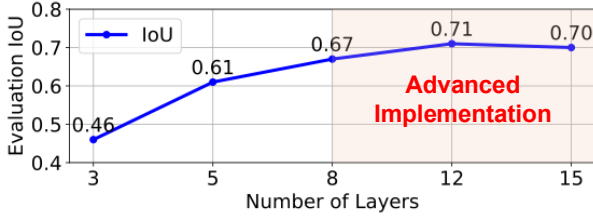


Fig. 3: The segmentation performance (IoU) of DONN models with different numbers of layers.

27.94 cm, i.e.,  $z = 27.94$  cm. A CMOS camera is placed at the end of the system to capture the output image. In this work, the loss function is formulated with MSE loss shown in Equation 11. For each task, the model is trained with 500 epochs with batch size of 64. All implementations are constructed using PyTorch v1.8.1. The experiments are conducted with Nvidia RTX A6000, while the simulated driving dataset with CARLA is collected with Nvidia 4090 Ti GPU.

#### B. Image Segmentation with CityScapes

This section provides the evaluation for the DONN system using CityScapes dataset, which contains 2975 training samples and 500 evaluation samples. As shown in Figure 2b, the input images in CityScapes are rich in environmental information including pedestrians, buildings, vehicles, and other urban elements. The DONN system is implemented with the system size of  $480 \times 480$ . The impact of the number of layers on segmentation performance is first explored in Section IV-B1. Further, the effects of different loss functions are explored in Section IV-B2, and the performance comparison with existing segmentation systems are provided in Section IV-B3 and Section IV-B3a. These evaluations are conducted using a 12-layer DONN system with three optical skip connections between the first three and last three layers.

1) **Image Segmentation Performance:** This section presents the performance evaluation of the DONN system using RGB images from the CityScapes dataset. Figure 3 shows the segmentation performance for DONN systems with depths ranging from 3 to 15 layers. With a 12-layer DONN system, the evaluation IoU is 0.71. While deeper architectures generally lead to improved performance, implementing DONN systems with more layers is challenging due to the exponential decay of light intensity for free-space propagation and the increased difficulty of optical alignment [4], [14]. Thus, more advanced optical devices and fabrication technology are required for stable and scalable hardware implementations of DONN systems, such as optoelectronic computing [40] and metasurface-enabled on-chip integration [18].

The normalized training loss curve and the evaluation IoU for a 12-layer DONN systems during the training process in shown in Figure 4. The visualizations of inference samples are shown in Figure 5a and Figure 10. Our model demonstrates strong confidence in segmenting prominent objects, such as buildings, from the sky and ground, when there is notable light contrast between the object and background. However, the

Input Image	RGB	RGB	RGB	Gray
Loss Function	MSE	BCE	Dice	MSE
IoU	0.70	0.66	0.66	0.36

TABLE I: Segmentation performance regarding IoU results on Cityscapes. We evaluate the model with different input image types and loss functions for comparison.

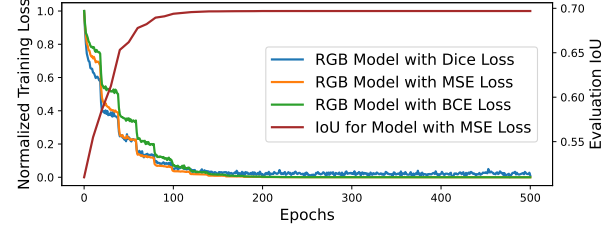


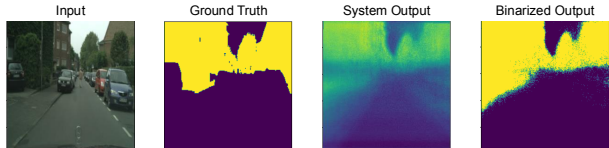
Fig. 4: Normalized training loss and evaluation IoU curve during training process.

model exhibits lower confidence in distinguishing fine details, such as segmenting vehicles from buildings. Additionally, some intricate features may be lost during the binarization process of the system outputs, potentially reducing segmentation precision.

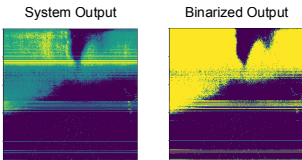
2) **Loss Function Comparison:** Moreover, the model are trained with different loss functions including (1) BCE loss, and (2) Dice loss. The normalized training loss curves for models with both loss functions are shown in Figure 4. The evaluation IoU with the model trained with BCE loss is 0.66 while the evaluation IoU with the model trained with Dice loss is 0.66, 4% lower IoU than the model trained with MSE loss, as shown in Table I. Additionally, the visualization sample for both models are provided in Figure 5b and Figure 5c. Compared to the system outputs from the model trained with MSE loss in Figure 5a, the other two models shows model-specific noise such as the horizontal noise line in Figure 5b with BCE loss, and the scatter noise cluster in Figure 5c with Dice loss.

3) **Single-Channel Model Comparison:** The RGB-channel system is further compared with the existing single-channel DONN system [14]. The single-channel DONN system is implemented with fifteen diffractive layers and three optical skip connections between corresponding layers as our RGB-channel system, while the input image to the single-channel DONN system is a gray-scale image. With the same training setups, the IoU of the single-channel DONN system is 0.36. A visualization sample is shown in Figure 6. Compared to our RGB-channel DONN system, the single-channel system exhibits 35% lower segmentation performance and shows less confidence during segmentation, as indicated by weaker light intensity contrast between the object and the background.

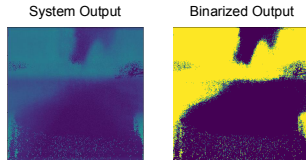
a) **Comparison with U-Net:** The RGB-channel DONN system is further compared with the digital U-Net [28]. The CityScapes dataset is pre-processed with binary classes and the input size is set as  $480 \times 480$  following the same dataset pre-processing as DONN systems. In the symmetric



(a) A visualization sample from the model trained with MSE loss.



(b) A visualization sample from the model trained with BCE loss.



(c) A visualization sample from the model trained with Dice loss.

Fig. 5: Visualization samples for RGB-channel DONN system trained with different loss functions. Both direct outputs from the DONN system and the binarized outputs are shown for comparisons.

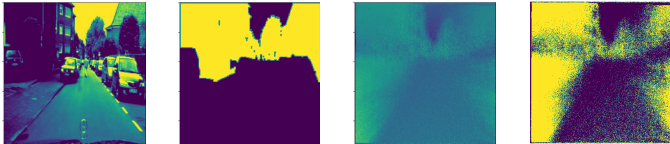


Fig. 6: A visualization sample with gray-scale input image for a single-channel DONN system.

encoder-decoder structure of the U-Net architecture<sup>1</sup>, the contracting path (encoder) captures context through repeated blocks of  $3 \times 3$  convolutions with ReLU activations and  $2 \times 2$  max pooling with stride 2 for downsampling. The initial number of filters for the convolution layers is 32. At each downsampling step, the number of feature channels is doubled. The expansive path (decoder) restores spatial detail via transposed convolutions and integrates fine-grained features from the encoder through skip connections, which directly link corresponding resolution levels between the two paths. A final  $1 \times 1$  convolutional layer maps the decoded feature maps to 2 output channels, generating the one-hot represented binary classes. The U-Net model is trained with BCE loss. The performance result is shown in Table II. The evaluation IoU for digital U-Net is 0.87, while our DONN system achieves the evaluation IoU performance of 0.71. The performance gap between digital neural networks and current DONNs suggests that existing DONNs trade off model performance for energy efficiency, highlighting the need for more advanced algorithms and optical implementations. The visualization of a evaluation sample from U-Net is shown in Figure 7.

### C. Lane Detection

In this section, we evaluate the DONN model for the lane detection task. In Section IV-C1, we evaluate the model using

<sup>1</sup><https://github.com/deepmancer/unet-semantic-segmentation>

TABLE II: Segmentation performance regarding F1 score, precision, recall results on CityScapes, compared with U-Net.

	F1 Score	Precision	Recall	IoU
RGB-channel DONN system	0.83	0.79	0.88	0.71
U-Net	0.93	0.93	0.94	0.87



Fig. 7: A visualization sample with U-Net model. The image from left to right corresponds to input image, groundtruth segmentation, and binarized system output.

a customized indoor dataset captured by a robotic vehicle (JETBOT<sup>2</sup>) navigating a real-world indoor track under uniform lighting conditions. A sample from the dataset is shown in Figure 2c. Then, in Section IV-C2, we evaluate the model with the simulated driving scenes using the CARLA simulator<sup>3</sup>. We collect data across different simulated maps with different weather conditions and times of the day for comprehensive evaluations of the model’s generalizability. A sample from the simulated driving dataset is shown in Figure 2d. The RGB-channel DONN model used for lane detections with both datasets is implemented with eight diffraction layers and three optical skip connections between the first three layers and the last three layers.

1) **Evaluations on Customized Indoor Track Dataset:** In this section, the model is evaluated with the customized indoor track dataset. The dataset is divided into training dataset with 4738 images and evaluation dataset with 1000 images. The RGB-channel DONN model is implemented with the system size of  $400 \times 400$  and trained with MSE loss. The average IoU for the evaluation dataset is 0.80. The visualized samples are shown in Figure 8, which shows that the proposed model can extract the track clearly in the indoor environment.

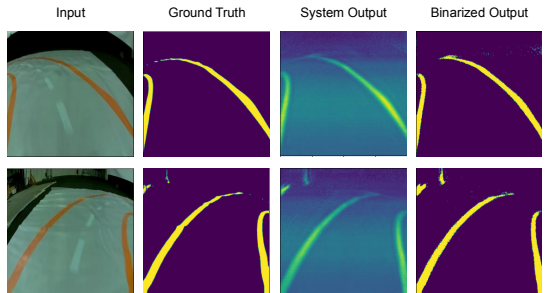
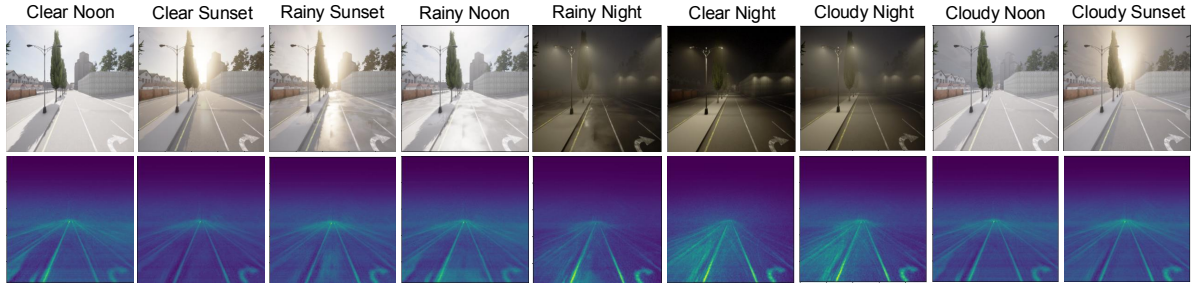


Fig. 8: The inference samples for lane detection with the customized indoor track dataset.

2) **Evaluations on Simulated Scenes in CARLA:** In this section, we further evaluate the generalizability of our RGB-channel DONN system with more complex dataset under

<sup>2</sup><https://jetbot.org/master/>

<sup>3</sup><https://carla.org>



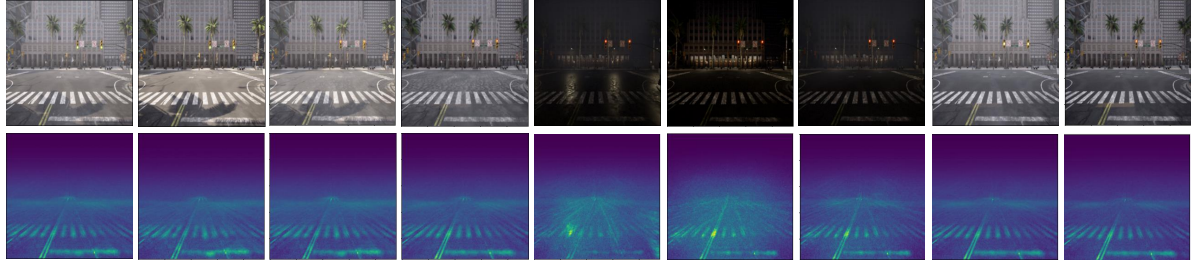
(a) The system outputs for lane detection in 'Map01' under different environmental conditions.



(b) The system outputs for lane detection in 'Map02' under different environmental conditions.



(c) The system outputs for lane detection in 'Map03' under different environmental conditions.



(d) The system outputs for lane detection in 'Map04' under different environmental conditions.

Fig. 9: The generalizability test of the proposed model with different maps under different environmental conditions.

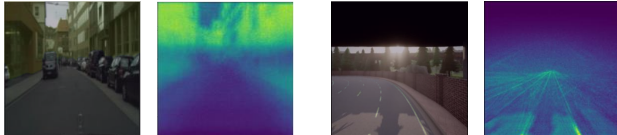


Fig. 10: DONN model is highly sensitive to light distribution. Light reflection and shadow can cause prediction noise.

diverse environmental conditions. The model is implemented with the system size of  $480 \times 480$ . Due to the extreme imbalance between the object and background, we implement the weighted binary cross-entropy loss to train the model as described in [12]. We first introduce the customized dataset generation by CARLA in Section IV-C2a, and we present the generalizability of the trained DONN model in Section IV-C2b

to different maps, weather conditions, and times of the day.

*a) Dataset Generation:* In this section, we introduce the details of the customized simulated driving dataset generated from simulations in CARLA. As shown in Figure 9, we collect samples from different maps, where 'Map01' and 'Map02' are used for training, while 'Map03' and 'Map04' are used for evaluations only, under different weather conditions, including 'Clear', 'Rainy', and 'Cloudy', at different times of the day, including 'Noon', 'Sunset', and 'Night'.

For training dataset, we collect 800 samples for each map under each environment condition including 'Clear' and 'Rainy' at 'Noon' and 'Sunset', 'DustStorm', and 'Default' weather conditions in the simulator. Thus, the total number of samples in the training dataset is  $6 \times 2 \times 800 = 9,600$ . For the evaluation dataset, we collect 200 samples for each

environment condition for all four maps, to evaluate the model's generalizability. Examples are shown in Figure 9.

*b) Generalizability Evaluation:* This section presents the evaluation of the trained DONN model to assess its generalizability across varying environments, including different maps, weather conditions, and times of day. The first four columns in Figures 9a and 9b show unseen samples with the same training maps and conditions. The model effectively detects lane markings, while showing high sensitivity to light distribution. For example, under 'Clear Noon', it identifies tree shadows, while, under 'Rainy Sunset,' it detects water reflections on the road, resulting in noise for lane detection.

**Generalizability to Different Maps** – As shown in the first four columns of 'Map03' and 'Map04' in Figures 9c and 9d, the model trained on 'Map01' and 'Map02' successfully detects lane markings in unseen maps.

**Generalizability to different weather conditions** – As shown in Figure 9, 'Clear' conditions exhibit direct illumination from the light source, with minimal diffuse reflection or attenuation in brightness. 'Rainy' conditions introduce water reflections on the road. 'Cloudy' conditions yield lower overall brightness and reduced lighting imbalance, particularly at sunset. As shown in the 'Cloudy Noon' and 'Cloudy Sunset' columns, the model trained on 'Clear' and 'Rainy' conditions successfully detects lane markings under 'Cloudy' weather.

**Generalizability to different time of the day** – As shown in the 'Night' columns in Figure 9, the model trained on 'Noon' and 'Sunset' successfully detects lane markings at 'Night'. 'Noon' conditions feature high overall brightness, leading to clear shadows and potentially ambiguous lane boundaries. 'Sunset' introduces a localized light source, causing uneven illumination. 'Night' conditions exhibit low overall brightness, with streetlights creating extreme lighting variations. For example, in 'Rainy Night' (Figures 9c and 9d), water reflections from streetlights introduce noise in model predictions.

## V. DISCUSSIONS

We propose a novel free-space all-optical DONN system for image processing in machine learning in this work. The general observations of the DONN model for image segmentation from our work indicate that the DONN model shows: (1) **High sensitivity to light distribution.** The DONN model's performance is highly influenced by the **uniformity of environmental lighting**. A more uniform light distribution generally leads to improved image processing performance as demonstrated from the comparisons between Section IV-C1 and Section IV-C2b, where the DONN model exhibits reduced noise and improved lane detection performance with the indoor track dataset. Moreover, the **high-contrast lighting distribution** such as water reflection and shadows, can confuse the model. As illustrated in Figures 10, reflections on building glass surfaces and the shadow on the road can result in noise for image segmentation. (2) **Necessity for improved post-processing optical binarization methods.** The diffraction process can cause uneven light distribution over the whole image. Although the system output preserves segmentation

boundaries, coarse binarization techniques can eliminate delicate segmentation details. **Developing a learnable model for adaptive post-processing tailored to varying outputs is critical to optical image segmentation.** Moreover, (3) **the hardware realization of DONN systems is critical for practical free-space all-optical computing**, which requires advanced design and fabrication technologies such as on-chip integration and optoelectronic computing [18], [40].

## VI. CONCLUSION

In this work, we propose a novel DONN architecture for RGB image processing, targeting tasks such as image segmentation and lane detection in autonomous driving systems. The model processes red ("R"), green ("G"), and blue ("B") components of a RGB image separately with all-optical computing channels, reducing ADC-related computational overhead and energy consumption by processing images in the optical domain. Furthermore, the DONN model offers high system throughput and ultrafast computation at the speed of light, making it a strong candidate for perception models in autonomous driving systems with power constraints for hardware deployments. We evaluate the model with image segmentation task using the Cityscapes dataset and lane detection task using customized indoor track dataset and CARLA-simulated driving dataset. We further evaluate the model's generalizability diverse environments, including different maps, weather conditions, and times of day with dataset from CARLA simulations, demonstrating its potential for real-world deployment in autonomous driving scenarios.

## REFERENCES

[1] CORDTS, M., OMTRAN, M., RAMOS, S., REHFELD, T., ENZWEILER, M., BENENSON, R., FRANKE, U., ROTH, S., AND SCHIELE, B. The cityscapes dataset for semantic urban scene understanding. In *Proceedings of the IEEE conference on computer vision and pattern recognition* (2016), pp. 3213–3223.

[2] DOSOVITSKIY, A., BEYER, L., KOLESNIKOV, A., WEISSENBORN, D., ZHAI, X., UNTERTHINER, T., DEHGHANI, M., MINDERER, M., HEIGOLD, G., GELLY, S., ET AL. An image is worth 16x16 words: Transformers for image recognition at scale. *arXiv preprint arXiv:2010.11929* (2020).

[3] DOSOVITSKIY, A., ROS, G., CODEVILLA, F., LOPEZ, A., AND KOLTUN, V. Carla: An open urban driving simulator. In *Conference on robot learning* (2017), PMLR, pp. 1–16.

[4] FU, T., ZHANG, J., SUN, R., HUANG, Y., XU, W., YANG, S., ZHU, Z., AND CHEN, H. Optical neural networks: progress and challenges. *Light: Science & Applications* 13, 1 (2024), 263.

[5] HE, K., ZHANG, X., REN, S., AND SUN, J. Deep residual learning for image recognition. In *Proceedings of the IEEE conference on computer vision and pattern recognition* (2016), pp. 770–778.

[6] HOWARD, A. G., ZHU, M., CHEN, B., KALENICHENKO, D., WANG, W., WEYAND, T., ANDRETTI, M., AND ADAM, H. Mobilenets: Efficient convolutional neural networks for mobile vision applications. *arXiv preprint arXiv:1704.04861* (2017).

[7] HU, J., MENGU, D., TZAROUCHIS, D. C., EDWARDS, B., ENGHETA, N., AND OZCAN, A. Diffractive optical computing in free space. *Nature Communications* 15, 1 (2024), 1525.

[8] HU, Y., YANG, J., CHEN, L., LI, K., SIMA, C., ZHU, X., CHAI, S., DU, S., LIN, T., WANG, W., ET AL. Planning-oriented autonomous driving. In *Proceedings of the IEEE/CVF conference on computer vision and pattern recognition* (2023), pp. 17853–17862.

[9] HUGHES, T. W., MINKOV, M., SHI, Y., AND FAN, S. Training of photonic neural networks through in situ backpropagation and gradient measurement. *Optica* 5, 7 (2018), 864–871.

[10] JIANG, M., BAI, Y., CORNMAN, A., DAVIS, C., HUANG, X., JEON, H., KULSHRESTHA, S., LAMBERT, J., LI, S., ZHOU, X., ET AL. Scenediffuser: Efficient and controllable driving simulation initialization and rollout. *Advances in Neural Information Processing Systems* 37 (2025), 55729–55760.

[11] KIRILOV, A., MINTUN, E., RAVI, N., MAO, H., ROLLAND, C., GUSTAFSON, L., XIAO, T., WHITEHEAD, S., BERG, A. C., LO, W.-Y., ET AL. Segment anything. In *Proceedings of the IEEE/CVF international conference on computer vision* (2023), pp. 4015–4026.

[12] LEE, D.-H., AND LIU, J.-L. End-to-end deep learning of lane detection and path prediction for real-time autonomous driving. *Signal, Image and Video Processing* 17, 1 (2023), 199–205.

[13] LI, Y., CHEN, R., RODRIGUEZ, B. S., GAO, W., AND YU, C. Multi-task learning in diffractive deep neural networks via hardware-software co-design. *Scientific Reports* (2021), 1–9.

[14] LIN, X., RIVENSON, Y., YARDIMCI, N. T., VELI, M., LUO, Y., JARRAHI, M., AND OZCAN, A. All-optical machine learning using diffractive deep neural networks. *Science* 361, 6406 (2018), 1004–1008.

[15] LIU, L., WANG, Y., AND SHI, W. Understanding time variations of dnn inference in autonomous driving. *arXiv preprint arXiv:2209.05487* (2022).

[16] LIU, W., RABINOVICH, A., AND BERG, A. C. Parsenet: Looking wider to see better. *arXiv preprint arXiv:1506.04579* (2015).

[17] LONG, J., SHELHAMER, E., AND DARRELL, T. Fully convolutional networks for semantic segmentation. In *Proceedings of the IEEE conference on computer vision and pattern recognition* (2015), pp. 3431–3440.

[18] LUO, X., HU, Y., OU, X., LI, X., LAI, J., LIU, N., CHENG, X., PAN, A., AND DUAN, H. Metasurface-enabled on-chip multiplexed diffractive neural networks in the visible. *Light: Science & Applications* 11, 1 (2022), 158.

[19] MENGU, D., LUO, Y., RIVENSON, Y., AND OZCAN, A. Analysis of diffractive optical neural networks and their integration with electronic neural networks. *IEEE Journal of Selected Topics in Quantum Electronics* 26, 1 (2019), 1–14.

[20] MENGU, D., RIVENSON, Y., AND OZCAN, A. Scale-, shift-, and rotation-invariant diffractive optical networks. *ACS photonics* 8, 1 (2020), 324–334.

[21] MILLETARI, F., NAVAB, N., AND AHMADI, S.-A. V-net: Fully convolutional neural networks for volumetric medical image segmentation. In *2016 Fourth International Conference on 3D Vision (3DV)* (2016), IEEE, pp. 565–571.

[22] MORA, L., WU, X., AND PANORI, A. Mind the gap: Developments in autonomous driving research and the sustainability challenge. *Journal of cleaner production* 275 (2020), 124087.

[23] MUHAMMAD, K., ULLAH, A., LLORET, J., DEL SER, J., AND DE ALBUQUERQUE, V. H. C. Deep learning for safe autonomous driving: Current challenges and future directions. *IEEE Transactions on Intelligent Transportation Systems* 22, 7 (2020), 4316–4336.

[24] NOH, H., HONG, S., AND HAN, B. Learning deconvolution network for semantic segmentation. In *Proceedings of the IEEE international conference on computer vision* (2015), pp. 1520–1528.

[25] NOOMWONGS, N., BAJPAI, A., PHUTTHABUREE, P., WONGPIYA, L., SKULTHAI, A., MAUNG, T. Z. B., MYINT, Y. M., ULLAH, I., WUTTISITTIKULJI, L., AND SAADI, M. Design and testing of autonomous steering system implemented on a toyota ha: Mo. In *2020 International Conference on Electronics, Information, and Communication (ICEIC)* (2020), IEEE, pp. 1–5.

[26] RAMEY, C. Silicon photonics for artificial intelligence acceleration: Hotchips 32. In *2020 IEEE hot chips 32 symposium (HCS)* (2020), IEEE Computer Society, pp. 1–26.

[27] RIZZOLI, G., BARBATO, F., AND ZANUTTIGH, P. Multimodal semantic segmentation in autonomous driving: A review of current approaches and future perspectives. *Technologies* 10, 4 (2022), 90.

[28] RONNEBERGER, O., FISCHER, P., AND BROX, T. U-net: Convolutional networks for biomedical image segmentation. In *International Conference on Medical image computing and computer-assisted intervention* (2015), Springer, pp. 234–241.

[29] SHEN, Y., HARRIS, N. C., SKIRLO, S., PRABHU, M., BAEHR-JONES, T., HOCHBERG, M., SUN, X., ZHAO, S., LAROCHELLE, H., ENGLUND, D., ET AL. Deep learning with coherent nanophotonic circuits. *Nature photonics* 11, 7 (2017), 441–446.

[30] SIMONYAN, K., AND ZISSERMAN, A. Very deep convolutional networks for large-scale image recognition. *arXiv preprint arXiv:1409.1556* (2014).

[31] SOLLI, D. R., AND JALALI, B. Analog optical computing. *Nature Photonics* 9, 11 (2015), 704–706.

[32] SUN, Y., DONG, M., YU, M., LIU, X., AND ZHU, L. Review of diffractive deep neural networks. *Journal of the Optical Society of America B* 40, 11 (2023), 2951–2961.

[33] TOBIN, M. S. Introduction to fourier optics. *American Scientist* 85, 6 (1997), 581–584.

[34] VASWANI, A., SHAZEER, N., PARMAR, N., USZKOREIT, J., JONES, L., GOMEZ, A. N., KAISER, L., AND POLOSUKHIN, I. Attention is all you need. *Advances in neural information processing systems* 30 (2017).

[35] WANG, C.-Y., YEH, I.-H., AND MARK LIAO, H.-Y. Yolov9: Learning what you want to learn using programmable gradient information. In *European conference on computer vision* (2024), Springer, pp. 1–21.

[36] WANG, S., XIA, C., LV, F., AND SHI, Y. Rt-detr3: Real-time end-to-end object detection with hierarchical dense positive supervision. *arXiv preprint arXiv:2409.08475* (2024).

[37] WU, B., IANDOLA, F., JIN, P. H., AND KEUTZER, K. Squeezedet: Unified, small, low power fully convolutional neural networks for real-time object detection for autonomous driving. In *Proceedings of the IEEE conference on computer vision and pattern recognition workshops* (2017), pp. 129–137.

[38] YAN, T., YANG, R., ZHENG, Z., LIN, X., XIONG, H., AND DAI, Q. All-optical graph representation learning using integrated diffractive photonic computing units. *Science Advances* 8, 24 (2022), eabn7630.

[39] YURTSEVER, E., LAMBERT, J., CARBALLO, A., AND TAKEDA, K. A survey of autonomous driving: Common practices and emerging technologies. *IEEE access* 8 (2020), 58443–58469.

[40] ZHOU, T., LIN, X., WU, J., CHEN, Y., XIE, H., LI, Y., FAN, J., WU, H., FANG, L., AND DAI, Q. Large-scale neuromorphic optoelectronic computing with a reconfigurable diffractive processing unit. *Nature Photonics* 15, 5 (2021), 367–373.